

GREEN AND FACILE SYNTHESIS OF CERIUM DOPED Ni₃Fe ELECTROCATALYST FOR EFFICIENT OXYGEN EVOLUTION REACTION

Farah Kanwal¹, Aisha Batool^{2*}, Rida Akbar¹, Sumreen Asim³ and Murtaza Saleem⁴

¹Institute of Chemistry, University of the Punjab, 54590-Lahore, Pakistan

²School of Physical Sciences, University of the Punjab, 54590-Lahore, Pakistan

³Khawaja Fareed University of Engineering and Information Technology, Department of
Chemistry, 64200-RYK, Pakistan

⁴Department of Physics, Syed Babar Ali School of Science and Engineering, Lahore University
of Management Sciences (LUMS), 54792-Lahore, Pakistan

(Received December 25, 2019; Revised March 13, 2020; Accepted March 14, 2020)

ABSTRACT. Electrochemical water splitting is the most promising pathway to produce high-purity hydrogen to alleviate global energy crisis. This reaction demands inexpensive, efficient and robust electrocatalyst for its commercial use. Herein, we demonstrate an effective, facile and scalable method for the synthesis of cerium doped Ni₃Fe nanostructures as an electrocatalyst for oxygen evolution reaction (OER) by following simple chemical bath deposition route. The different molar ratios (3, 6 and 12 mM) of cerium in the chemical bath were used to study its effect on the structural and the electrochemical properties of the Ni₃Fe nanostructured films. Doping of cerium contents induced variations in the morphology of deposited Ni₃Fe nanostructures. The optimized electrocatalyst Ni₃Fe/Ce-6 yielded high surface area catalyst nanosheets uniformly deposited on three-dimensional conductive scaffold to ensure increase in the exposure of doped Ni₃Fe catalytic sites with high electrical conductivity. As a result, this earth-abundant electrocatalyst affords high OER performance with a small overpotential of 310 mV versus reversible hydrogen electrode (RHE) at 10 mA cm⁻² and retains good stability up to ~ 10 h in alkaline electrolyte. This scalable strategy has great potential in future advancement of efficient and low-cost electrocatalysts for their large-scale application in energy conversion systems.

KEY WORDS: Oxygen evolution, Electrocatalyst, Ni₃Fe nanostructures, Cerium, Alkaline electrolyte

INTRODUCTION

Splitting of water is the most promising pathway to get hydrogen as green energy carrier, to address the energy crisis across the globe due to diminishing fossil fuels. Water splitting is classified into two half reactions: the oxygen evolution reaction (OER) at the anode; and hydrogen evolution reaction (HER) at the cathode. OER is the bottleneck reaction in the water splitting and it involves many reaction intermediates and barriers ($4\text{OH}^- \rightarrow 2\text{H}_2\text{O} + 4\text{e}^- + \text{O}_2$) during the anodic polarization process; and hence need large overpotential above the thermodynamic requirement of 1.23 V. For commercial use, the highly efficient OER electrocatalyst as key component of the water electrolyser is crucial to accelerate the reaction kinetics and to effectively lower the overpotential for energy conversion [1-4]. Currently, the state-of-the-art electrocatalysts to fulfil the technological requirements are IrO₂ and RuO₂ for OER. But the scarcity and the high cost of these noble metals are major barriers for their implementation at large scale. Motivated by these challenges with non-renewable resources of energy and the noble metals based electrocatalysts, tremendous research has been conducted in this field in the development of advanced renewable technologies with inexpensive electrocatalyst systems that are highly active and robust for water oxidation [5-12].

Among all non-noble metals alternatives, NiFe-based electrocatalysts have appeared to be potential candidates with eco-friendly property and high electrocatalytic activity in alkaline electrolyte [1, 7, 13-20]. The OER activity, in general, depends on the high oxidation states and

*Corresponding author. E-mail: dr.batool.aisha@gmail.com

This work is licensed under the Creative Commons Attribution 4.0 International License

the catalytic active sites in the transition metal elements [21-26]. The third element doping from 3d transition metals can modify the electronic structure of NiFe-based electrocatalysts by introduction of defects to facilitate the reaction intermediates with low reaction barriers for OER [27, 28]. Recently several groups reported the introduction of cerium in the host catalyst with modified electronic structure for improved OER performance. For instance, CeO₂ doping in Ni(OH)₂ shows great contribution in the enhancement of OER owing to strong electronic interaction between these two phases [29]. The introduction of cerium induced crystal structure amorphourization of CoO_x with increased cerium related oxygen storage capacity. These modifications lead to increase in electrochemical surface area of nanostructures and consequently high intrinsic OER activity of the resultant catalyst [30]. The promotion of NiFe-LDH for significantly enhanced OER activity by doping with cerium and interfaced with CNTs to form hierarchical nanocomposite has been demonstrated due to induced lattice defects, flexible coordination number of Ce³⁺ and strongly coupled interface [31]. Although various strategies have been adopted to introduce cerium into host catalyst, however, a scalable, cost-effective and simple synthetic protocol with precise control over the growth of trimetallic electrocatalyst without coalescence of nanostructures on conductive scaffolds is rare. The self-aggregation of catalyst nanostructures causes blockage of the active sites due to accumulation of generated gas bubbles that obstructed the diffusion of both reactants and products, which is the major source to increase the overpotential [23, 25].

In this work, we demonstrate an effective, facile and inexpensive strategy for synthesis of cerium doped NiFe-based electrocatalyst nanosheets. Our strategy has following key features (1) amorphous phase of cerium in the host catalyst and dramatic variations in Ni₃Fe morphology, (2) the nucleation of homogeneous deposition of electrocatalyst nanosheets with more accessible catalytic sites, and (3) the superior performance of cerium doped catalyst in catalyzing the OER in comparison to control sample of Ni₃Fe. Thus, our low-cost and simple strategy developed an electrocatalyst that affords superior water oxidation activity with a low over potential of 310 mV_{RHE} at 10 mA cm⁻² and a good stability in alkaline electrolyte.

EXPERIMENTAL

Materials

Hydrochloric acid (HCl), ethanol, iron sulfate heptahydrate (FeSO₄·7H₂O), cerium nitrate (Ce(NO₃)₃·6H₂O), trisodium citrate dehydrate (Na₃C₆H₅O₇) and Ni foam were used. Deionized water, paraffin oil were the materials required for carrying out the synthesis. All chemicals were of lab grade and were utilized without any purification.

Experimental details

Prior to synthesis, pieces of Ni foam (1 cm × 3 cm) were washed with 3 M HCl solution, deionized water and ethanol in succession, each for 10 min in ultrasonic bath to remove any oxide layer. The chemical bath solutions with different atomic ratio of Fe to Ce were prepared by mixing 50 mmol of FeSO₄·7H₂O and 3 mM of Na₃C₆H₅O₇ with varied contents of Ce(NO₃)₃·6H₂O (i.e., 3, 6 and 12 mM) in 100 mL of deionized water and stirred them for 0.5 h. The cleaned pieces of Ni foam were inserted in the above prepared solutions followed by the oil bath heating at 90 °C for the development of different products and named as Ni₃Fe/Ce-3, Ni₃Fe/Ce-6 and Ni₃Fe/Ce-12, respectively.

For the synthesis of control sample Ni₃Fe, the method is similar to that of all above cerium doped Ni₃Fe but without adding Ce(NO₃)₃·6H₂O into the chemical bath solution. After deposition, all prepared products were washed with deionized water and ethanol; and then dried at 60 °C overnight.

Structural characterization techniques

X-ray diffraction (XRD) patterns were obtained from X'pert powder diffractometer using CuK α radiations ($\lambda = 0.15418$ nm) with an operating voltage of 40 kV and an operating current of 40 mA at the scan rate of $0.05^\circ 2\theta$ s⁻¹. Field emission scanning electron microscope (FESEM, Hitachi, Japan) at an accelerating voltage of 10 kV was employed for morphology analysis of Ni₃Fe, Ni₃Fe/Ce-3, Ni₃Fe/Ce-6 and Ni₃Fe/Ce-12 films on the Ni foam surface.

Electrochemical measurements

To evaluate the electrocatalytic performance of synthesized electrode materials for oxygen evolution reaction (OER), a number of electrochemical measurement techniques were employed. Generally, the techniques involve the recording of electric response of the catalyst to an applied potential. From this current potential behavior, salient electrochemical properties such as overpotential and Tafel slope were extracted out.

All electrochemical measurements were performed in alkaline electrolyte (1.0 M KOH, pH 13.6) using 3-electrode cell was used to carry out these measurements. That system comprises of working, counter electrode and reference electrodes for the purpose of completion of the electrical circuit. All the electrochemical activities were conducted on a Zahner Zennium electrochemical workstation at a sweep rate of 50 mV.s⁻¹.

In our study, Pt sheet was employed as the counter electrode, saturated calomel electrode (SCE) as the reference electrode and synthesized samples were as working electrodes, in dark. For the conversion of potential against the reversible hydrogen electrode (RHE) from the SCE, following equation is used:

$$E_{\text{RHE}} = E_{\text{SCE}} + 0.244 \text{ V} + 0.059 \times \text{pH}. \quad (1)$$

Linear sweep voltammetry (LSV) technique was used to determine the current response as a result of applied voltage. This technique involves the unidirectional voltage sweep from an initial potential to final potential. LSV were corrected for OER with ohmic drop using relation:

$$V_{\text{R}} = V_{\text{app}} - iR_{\text{s}}, \quad (2)$$

where V_{app} is the applied potential and R_{s} is the solution resistance.

The electrocatalytic performance of the electrode either for OER is evaluated by Tafel slope. Tafel plot was calculated from the corresponding LSV polarization curves and it account for the changes in mechanism at different overpotentials. Tafel slope determines current response of the system to the applied voltage (V) and can be calculated by using following equation 3:

$$\eta = a + b \log(j) \quad (3)$$

where η represents the overpotential, b is the Tafel slope in mV.dec⁻¹, j being the current density. Low Tafel slope and large current density indicate the efficient performance. The overpotential was calculated by using the following relation:

$$E(\eta) = E(\text{SCE}) + 0.244 + (0.059 \times \text{pH}) - 1.23, \quad (4)$$

The electrochemical active surface area (ECSA) of electrodes CF, t-CF and NiFe@t-CF were calculated from the electrochemical double layer capacitance (C_{dl}). The scan-rate (v) dependent capacitive current, I_{c} is associated with the C_{dl} according to relation:

$$\text{ECSA} = C_{\text{dl}} = I_{\text{c}}/v \quad (5)$$

where $I_{\text{c}} = I_{\text{anodic}} - I_{\text{cathodic}}$, calculated in the middle of potential domain as a function of scan rate v , that yielded a linear slope equal to $2 \times C_{\text{dl}}$.

Electrochemical impedance spectroscopy (EIS) is a versatile tool to evaluate the electrochemical response of a system to an applied alternating potential. EIS is basically employed to determine the resistance of the electrode reaction due to the transfer of charges R_{CT} . The EIS measurements were carried out at 1.45 V_{RHE} . The frequency scan range was from 100 kHz to 0.1 Hz with the amplitude of the sinusoidal wave 10 mV.

RESULTS AND DISCUSSION

Oxygen evolution reaction (OER) is energetically the most inefficient part of the water electrolysis $4OH^- \rightarrow 2H_2O + O_2 + 4e^-$. Chemical bath deposition route was adopted as a green, scalable, facile and low-cost synthesis route. The synthesis was initially monitored by the color change of Ni foam from silvery white to brownish yellow (Figure 1a). Ni foam was employed as a conductive substrate and assisted as the source of nickel (Ni) in the reaction. During the synthesis process Fe^{+2} oxidize into Fe^{+3} and Fe^{+4} , then oxidization of Ni foam to obtain Ni^{+2} . While cerium doping facilitates effectively to modulate the morphology of the as-grown catalyst nanostructures by increasing cerium related oxygen storage capacity [32, 33].

X-Ray diffraction (XRD)

The as-synthesized films were characterized by XRD (Figure 1b). The presence of diffraction peaks at 44.2° , 51.4° , and 75.7° corresponding to diffraction plans of (111), (200) and (311), respectively, indicated the formation of Ni_3Fe (JSPDS card no: 48-0419). No other obvious crystallization peaks were observed with the exception of the diffraction peaks associated with Ni_3Fe . This analysis evident that the cerium phase in the as-synthesized electrocatalyst samples is amorphous; and this strongly suggests that they are likely small grain (oxy)hydroxide phases at OER potentials [34].

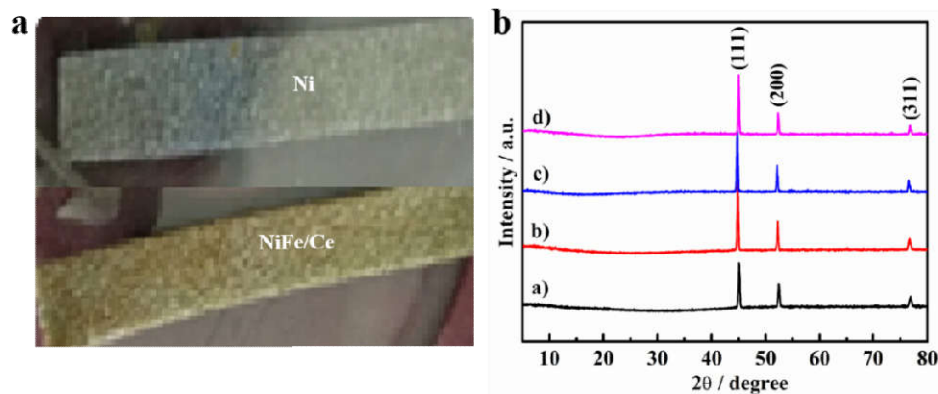


Figure 1. (a) Digital photograph showing the color change of Ni foam from silvery white to brownish yellow after deposition of electrocatalyst film. (b) XRD patterns of (a) Ni_3Fe , (b) $Ni_3Fe/Ce-3$, (c) $Ni_3Fe/Ce-6$ and (d) $Ni_3Fe/Ce-12$.

Field emission scanning electron microscopy-energy dispersive X-ray spectroscopy (SEM-EDX) analysis

The morphologies of the as-grown catalyst structures were investigated by field-emission scanning electron microscopy (SEM). In Figure 2a, the SEM image of Ni_3Fe shows that without

the incorporation of Ce during synthesis, the catalyst film exhibits no distinct morphology and is apparently less porous. The electrode sample Ni₃Fe/Ce-3 shows better morphology in comparison to sample Ni₃Fe. Figure 2b illustrates the homogeneous dispersion of small globules mounted vertically on the surface of Ni foam. However, there is no full coverage of these globular structures on the 3D scaffold of Ni. SEM images of Ni₃Fe/Ce-6 (Figure 2c) clearly reveal that the entire surface of globules on Ni scaffold is homogeneously covered with densely vertically aligned nanosheets. The nanoplatelet morphology with cavities in between the nanowalls exhibits high surface area and porosity. Such open nanosheets architecture built by Ni₃Fe/Ce-6 afford high surface area and more exposed catalytic active sites, an easy of electrolyte penetration and fast adsorption and desorption of the generated gas bubbles to facilitate OER activity. While Figure 2d presents the globular nanoparticles morphology of Ni₃Fe/Ce-12 with rough surface that are stacked over each other on the conductive surface of Ni template. The catalyst particles are homogeneously dispersed on 3D network of Ni foam. The SEM analysis of all samples indicated that Ce contents played vital role to modulate the morphology of the grown nanostructures. The different morphologies offer different geometrical characteristics and enhancement in the OER performance. Ce loading may create a synergistic effect by perturbing the electronic structure of the host catalyst Ni₃Fe surface and the number of exposed active sites on the surface of catalyst [29, 30].

As no diffraction peak is observed in Ni₃Fe/Ce-6 to confirm the presence of cerium may be due to the amorphization of the cerium related phase in the deposited electrocatalyst film. So we perform its EDX to confirm the presence of Ce contents in the Ni₃Fe/Ce-6 deposited electrocatalyst film. The EDX spectrum of Ni₃Fe/Ce-6 confirmed the presence of O, Ni, Fe and Ce elements in Figure 2e. In addition, the inset table in Figure 2e shows the percentages of these elements. The ratios of Ni/Fe and Ni/Ce are found to be 3 and 1.5, respectively, for Ni₃Fe/Ce-6.

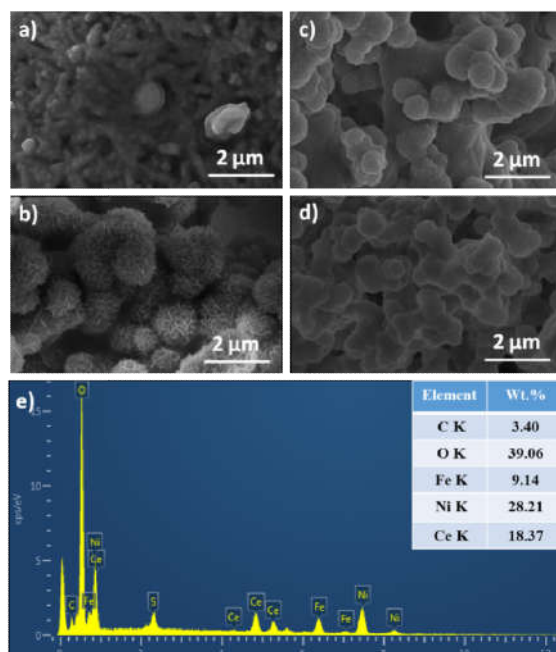


Figure 2. SEM images of (a) Ni₃Fe, (b) Ni₃Fe/Ce-3, (c) Ni₃Fe/Ce-6 and (d) Ni₃Fe/Ce-12 at 25 kX; and (e) the corresponding EDX spectrum of Ni₃Fe/Ce-6.

Electrochemical measurements

The electrochemical properties of developed cerium doped Ni₃Fe nanostructures deposited directly on the porous 3D scaffold of the conductive Ni foam towards OER were unveiled with the help standard analytical methods such as linear sweep voltammetry (LSV), Tafel plots and electrochemical impedance spectroscopy (EIS). The potentials were measured versus saturated calomel electrode (SCE) and are reported here versus reversible hydrogen electrode (RHE).

Linear sweep voltammetry (LSV)

The catalytic activities of the electrocatalysts towards OER are compared based on three key parameters deduced from the LSV curves are the onset potential, minimum potential required to attain a current density of 10 mA.cm⁻² and overpotential. The electrode samples Ni₃Fe, Ni₃Fe/Ce-3, Ni₃Fe/Ce-6 and Ni₃Fe/Ce-12 exhibit the onset potentials of 1.55, 1.53, 1.48 and 1.51 V_{RHE}, respectively. The minimum potential to reach current density of 10 mA.cm⁻² was 1.62, 1.57, 1.54 and 1.58 V_{RHE}, respectively. The same trend was observed for the over potentials and was 0.39, 0.37, 0.31 and 0.35 V_{RHE} for the Ni₃Fe, Ni₃Fe/Ce-3, Ni₃Fe/Ce-6 and Ni₃Fe/Ce-12, respectively. The material sample Ni₃Fe/Ce-6 showed the superior catalytic performance among all samples in 1.0 M KOH electrolyte. The efficient intrinsic OER activity is owing to high surface area offered by nanoplatelet morphology of Ni₃Fe/Ce-6 with more accessible active sites for the reactants as evident from its SEM images.

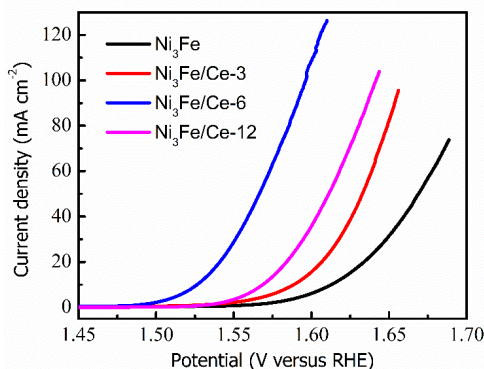


Figure 3. LSV curves (with iR correction) of Ni₃Fe (black curve), Ni₃Fe/Ce-3 (red curve), Ni₃Fe/Ce-6 (blue curve) and Ni₃Fe/Ce-12 (magenta curve) in 1.0 M KOH electrolyte.

Tafel slope

To achieve the more insight into OER performance of the prepared catalysts samples, Tafel plots were calculated. Tafel plots for all catalyst samples were generated by plotting the log of current density ($\log I$) against applied potentials (V_{SCE}). The Tafel slope (b) was extracted by fitting the linear portion of the plots to the Tafel equation as described in equation 3. Figure 4 displays the Tafel slopes of all electrodes derived from their respective LSV curves by fitting the linear portion of their Tafel plots into the Tafel equation ($\eta = a + b \log [j]$) to show the influence of the overpotential on the current density to evaluate their OER kinetics. It is found that Ni₃Fe/Ce-6 shows smallest Tafel slope of 49 mV dec⁻¹ among all four electrocatalyst samples representing more favorable reaction kinetics due to higher inherent OER activity of this as-synthesized electrocatalyst sample. Tafel slopes of 58, 55 and 51 mV/decade were observed for the samples Ni₃Fe, Ni₃Fe/Ce-3, and Ni₃Fe/Ce-12, respectively. The results indicate

that the optimal loading of the Ce during synthesis lead to the more favorable reaction kinetics. The electrocatalytic mechanism of the OER is complicated and OER performance relates with the number of catalytic active sites (M) and adsorption affinity of H₂O, *OH, *O, MOOH and MOO⁻ as the reaction intermediates. Generally, it proceeds in the following multistep reactions under alkaline condition⁴¹:



Every step from Eq. 1-4 is assumed to be the rate determining to define the electric current. Based on the microkinetic analysis for the correlation of Tafel slope and the rate determining step, Eq. 4 should be the rate determining step for the Ni₃Fe/Ce-3 since its Tafel slope is 55 mV dec⁻¹ [35].

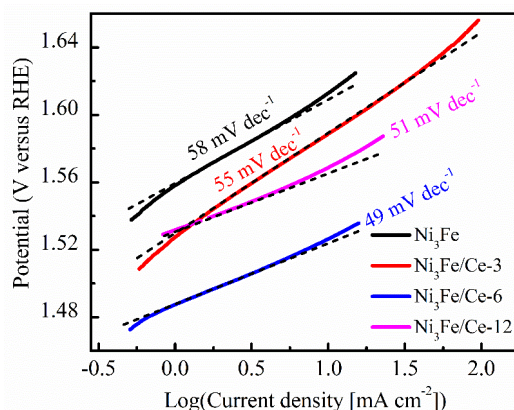


Figure 4. Tafel plots of Ni₃Fe (black curve), Ni₃Fe/Ce-3 (red curve), Ni₃Fe/Ce-6 (blue curve) and Ni₃Fe/Ce-12 (magenta curve) derived from the corresponding LSV curves of OER.

Electrochemical impedance spectroscopy (EIS)

Further, electrochemical impedance spectroscopy (EIS) was carried out to study the electrocatalytic behavior of Ni₃Fe, Ni₃Fe/Ce-3, Ni₃Fe/Ce-6 and Ni₃Fe/Ce-12. Nyquist plots were obtained from Ni₃Fe, Ni₃Fe/Ce-3, Ni₃Fe/Ce-6 and Ni₃Fe/Ce-12 electrocatalysts deposited on the porous 3D structure of Ni foam are shown in the Figure 5. These plots showing two semicircles corresponding to the charge transfer resistance at the anode/electrolyte interface and in the anode, respectively. The high-frequency semicircle for the Ni₃Fe/Ce-6 is smallest indicating the enhanced charge transport with very less charge transfer resistance (R_{ct}) of $\sim 2.63 \Omega$ in comparison to Ni₃Fe ($\sim 12 \Omega$), Ni₃Fe/Ce-3 ($\sim 4.58 \Omega$) and Ni₃Fe/Ce-12 ($\sim 3.76 \Omega$). It also demonstrates the higher conductivity and the good electrical contact between the conducting scaffold of Ni and the deposited Ni₃Fe nanoplatelets in Ni₃Fe/Ce-6.

Electrochemical active surface area (ECSA) measurements

Figure 6(a-c) show the cyclic voltammetry (CV) curves for pristine Ni and the optimized electrocatalyst Ni₃Fe/Ce-6 in the non-Faradaic potential region from 0.10 to 0.20 V in 1.0 M

KOH solution. Where for these CV measurements, CV curves were run at multiple scan rates (v) of 20, 40, 60, 80 and 100 mV s^{-1} . The plot of capacitive current (I_c) at the middle of the applied potential window versus v gives C_{dl} that has direct relation with ECSA as given in Equation 5. Figure 6c shows that $\text{Ni}_3\text{Fe}/\text{Ce}-6$ exhibits the 3.5 times higher ECSA (3.52 mF cm^{-2}) in comparison to pristine Ni foam (0.98 mF cm^{-2}). The large ECSA is resulting from the high surface area catalyst nanosheets of $\text{NiFe}@t\text{-CF}$ uniformly deposited on Ni foam surface as inferred in its SEM images.

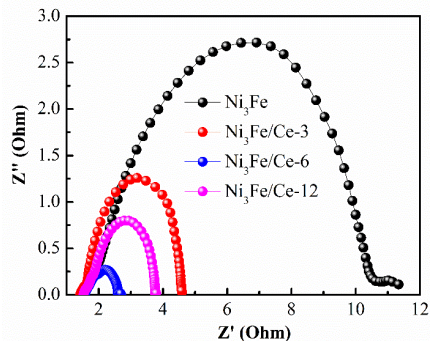


Figure 5. Nyquist plots of Ni_3Fe (black curve), $\text{Ni}_3\text{Fe}/\text{Ce}-3$ (red curve), $\text{Ni}_3\text{Fe}/\text{Ce}-6$ (blue curve) and $\text{Ni}_3\text{Fe}/\text{Ce}-12$ (magenta curve).

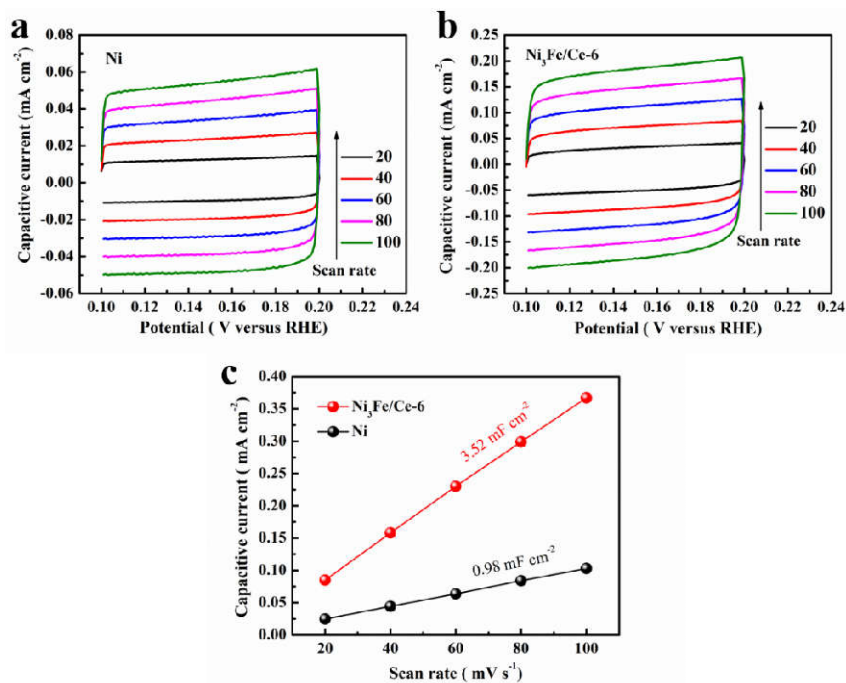


Figure 6. CV curves in non-Faradaic region in 1.0 M KOH for a) pristine Ni foam and b) $\text{Ni}_3\text{Fe}/\text{Ce}-6$. c) Calculated C_{dl} plots of Ni (black curve) and $\text{Ni}_3\text{Fe}/\text{Ce}-6$ (red line).

Chronoamperometric measurements

As stability is an important parameter to evaluate the feasibility of the material for practical applications. The long-term stability of optimized electrocatalyst was examined by the chronoamperometry response at 1.54 V in 1.0 M KOH solution. As shown in Figure 6, Ni₃Fe/Ce-6 retains its current density up to 10 h (36,000 s) of continuous operation with slight degradation in the value of its original current density (~9.8 mA cm⁻²), suggesting its good operational stability in the alkaline solution.

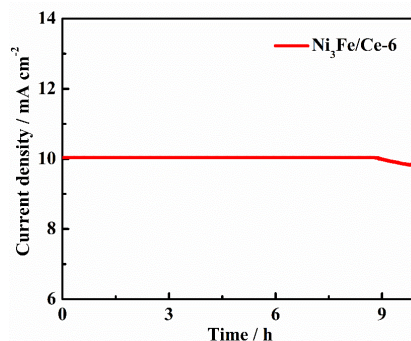


Figure 7. Chronoamperometric test of Ni₃Fe-6 at 1.54 V_{RHE}.

CONCLUSION

In conclusion, we have used a facile, simple and effective strategy for the synthesis of Ni₃Fe as highly efficient electrocatalyst for OER in the alkaline media. Their morphology can be effectively tuned by the doping of cerium. Different doping percentages of cerium effectively tuned the morphology to form nanoparticles, globules and nanoplatelets. The high OER activity of the optimum sample attributed to the high surface area with more exposed active catalytic sites, low charge transfer resistance between the electrocatalyst and electrolyte solution owing to the non-aggregated morphology of deposited nanostructures. Considering the efficiency of our synthesized electrocatalyst, the present study will undoubtedly open opportunities for the development of non-precious and high performance electrocatalysts by adopting a simple synthetic route at moderate temperature.

ACKNOWLEDGEMENT

This research work was supported by the Higher Education Commission (HEC), Islamabad, Pakistan.

REFERENCES

1. Abe, J.O.; Popoola, A.P.I.; Ajenifuja, E.; Popoola, O.M. Hydrogen energy, economy and storage: Review and recommendation. *Int. J. Hydrogen Energ.* **2019**, *44*, 15072-15086.
2. Hosseini, S.E.; Wahid, M.A. Hydrogen production from renewable and sustainable energy resources: Promising green energy carrier for clean development. *Renew. Sust. Energ. Rev.* **2016**, *57*, 850-866.
3. McCrory, C.C.; Jung, S.; Ferrer, I.M.; Chatman, S.M.; Peters, J.C.; Jaramillo, T.F. Benchmarking hydrogen evolving reaction and oxygen evolving reaction electrocatalysts for solar water splitting devices. *J. Am. Chem. Soc.* **2015**, *137*, 4347-4357.

4. Zhao, Y.; Nakamura, R.; Kamiya, K.; Nakanishi, S.; Hashimoto, K. Nitrogen-doped carbon nanomaterials as non-metal electrocatalysts for water oxidation. *Nat. Commun.* **2013**, *4*, 1-6.
5. Ouattara, L.; Diaco, T.; Bokra, Y. Influence of water on the anodic oxidation mechanism of diethylenetriamine (deta) on platinum electrode. *Bull. Chem. Soc. Ethiop.* **2015**, *20*, 269-277.
6. Boye, B.; Brillas, E.; Marselli, B.; Michaud, P.-A.; Comminellis, C.; Dieng, M.M. Electrochemical decontamination of waters by advanced oxidation processes (aops): Case of the mineralization of 2,4,5-t on bdd electrode. *Bull. Chem. Soc. Ethiop.* **2004**, *18*, 205-214.
7. Getachew, T.; Addis, F.; Beyene, T.; Mehretie, S.; Admassie, S. Amino-substituted naphthalene sulfonic acid/graphene composite as metal-free catalysts for oxygen reduction reactions. *Bull. Chem. Soc. Ethiop.* **2019**, *33*, 359-372.
8. Ye, Z.; Li, T.; Ma, G.; Dong, Y.; Zhou, X. Metal-ion (Fe, V, Co, and Ni)-doped MnO₂ ultrathin nanosheets supported on carbon fiber paper for the oxygen evolution reaction. *Adv. Funct. Mater.* **2017**, *27*, 1704083.
9. Yousaf, M.; Chen, Y.; Tabassum, H.; Wang, Z.; Wang, Y.; Abid, A.Y.; Gao, P. A dual protection system for heterostructured 3D CNT/CoSe₂/C as high areal capacity anode for sodium storage. *Adv. Sci.* **2020**, *5*, 1902907.
10. Yousaf, M.; Wang, Y.; Chen, Y.; Wang, Z.; Firdous, A.; Ali, Z.; Han, R.P.S. A 3D trilayered CNT/MoSe₂/C heterostructure with an expanded MoSe₂ interlayer spacing for an efficient sodium storage. *Adv. Energy Mater.* **2019**, 1900567.
11. Yousaf, M.; Wang, Y.; Chen, Y.; Wang, Z.; Aftab, W.; Mahmood, A.; Han, R.P.S. Tunable free-standing core-shell CNT@MoSe₂ anode for lithium storage. *ACS Appl. Mater.* **2018**, *10*, 14622-14631.
12. Yousaf, M.; Shi, H.T.H.; Wang, Y.; Chen, Y.; Ma, Z.; Cao, A.; Han, R.P.S. Novel pliable electrodes for flexible electrochemical energy storage devices: recent progress and challenges. *Adv. Energy Mater.* **2016**, *6*, 1600490.
13. Hu, F.; Zhu, S.; Chen, S.; Li, Y.; Ma, L.; Wu, T.; Zhang, Y.; Wang, C.; Liu, C.; Yang, X.X. Amorphous metallic NiFeP - A conductive bulk material achieving high activity for oxygen evolution reaction in both alkaline and acidic media. *Adv. Mater.* **2017**, *29*, 1606570.
14. Zhan, T.; Liu, X.; Lu, S.; Hou, W. Nitrogen doped NiFe layered double hydroxide-reduced graphene oxide mesoporous nanosphere as an effective bifunctional electrocatalyst for oxygen reduction and evolution reactions. *Appl. Catal. B: Environ.* **2017**, *205*, 551-558.
15. Dionigi, F.; Strasser, P. NiFe-based (oxy)hydroxide catalysts for oxygen evolution reaction in non-acidic electrolytes. *Adv. Energy Mater.* **2016**, *6*, 1600621.
16. Cheng, Y.; Jiang, S.P. Materials Int-advances in electrocatalysts for oxygen evolution reaction of water electrolysis-from metal oxides to carbon nanotubes. *Proc. Nat. Sci. Mater.* **2015**, *25*, 545-553.
17. Yu, X.; Yang, P.; Chen, S.; Zhang, M.; Shi, G. NiFe alloy protected silicon photoanode for efficient water splitting. *Adv. Energy Mater.* **2017**, *7*, 1601805.
18. Stevens, M.B.; Trang, C.D.; Enman, L.J.; Deng, J.; Boettcher, S.W. Reactive Fe-sites in NiFe (oxy)hydroxide are responsible for exceptional oxygen electrocatalysis activity. *J. Am. Chem. Soc.* **2017**, *139*, 11361-11364.
19. Deng, J.; Nellist, M.R.; Stevens, M.B.; Dette, C.; Wang, Y.; Boettcher, S.W. Morphology dynamics of single-layered Ni(OH)₂-NiOOH nanosheets and subsequent Fe incorporation studied by in situ electrochemical atomic force microscopy. *Nano Lett.* **2017**, *17*, 6922-6926.
20. Ma, W.; Ma, R.; Wang, C.; Liang, J.; Liu, X.; Zhou, K.; Sasaki, T. A superlattice of alternately stacked Ni-Fe hydroxide nanosheets and graphene for efficient splitting of water. *ACS Nano.* **2015**, *9*, 1977-1984.
21. Gong, M.; Li, Y.; Wang, H.; Liang, Y.; Wu, J.Z.; Zhou, J.; Wang, J.; Regier, T.; Wei, F.; Dai, H. An advanced Ni-Fe layered double hydroxide electrocatalyst for water oxidation. *J. Am. Chem. Soc.* **2013**, *135*, 8452-8455.

22. Raj, I.A.; Vasu, K. Transition metal-based hydrogen electrodes in alkaline solution-electrocatalysis on nickel based binary alloy coatings. *J. Appl. Electrochem.* **1990**, *20*, 32-38.
23. Chen, Z.; Cummins, D.; Reinecke, B.N.; Clark, E.; Sunkara, M.K.; Jaramillo, T.F. Core-shell MoO₃-MoS₂ nanowires for hydrogen evolution-A functional design for electrocatalytic materials. *Nano Lett.* **2011**, *11*, 4168-4175.
24. Song, H.; Oh, S.; Yoon, H.; Kim, K.-H.; Ryu, S.; Oh, J. Bifunctional NiFe inverse opal electrocatalysts with heterojunction Si solar cells for 9.54%-efficient unassisted solar water splitting. *Nano Energ.* **2017**, *42*, 1-7.
25. Liu, J.; Zheng, Y.; Wang, Z.; Lu, Z.; Vasileff, A.; Qiao, S.-Z. Free-standing single-crystalline NiFe-hydroxide nanoflake arrays - A self-activated and robust electrocatalyst for oxygen evolution. *Chem. Commun.* **2018**, *54*, 463-466.
26. Suryanto, B.H.; Zhao, C. Surface-oxidized carbon black as a catalyst for the water oxidation and alcohol oxidation reactions. *Chem. Commun.* **2016**, *52*, 6439-6444.
27. Holade, Y.; Servat, K.; Tingry, S.; Napporn, T.W.; Remita, H.; Cornu, D.; Kokoh, K.B. Advances in electrocatalysis for energy conversion and synthesis of organic molecules. *ChemPhysChem.* **2017**, *18*, 2573-2605.
28. Fang, G.; Cai, J.; Huang, Z.; Zhang, C. One-step electrodeposition of cerium-doped nickel hydroxide nanosheets for effective oxygen generation. *RSC Adv.* **2019**, *9*, 17891-17896.
29. Du, X.; Zhang, D.; Ruihua, L.S.; Zhang, J. Morphology dependence of catalytic properties of Ni/CeO₂ nanostructures for carbon dioxide reforming of methane. *Phys. Chem. C* **2012**, *116*, 10009-10016.
30. Xu, S.; Lv, C.; He, T.; Huang, Z.; Zhanga, C. Amorphous film of cerium doped cobalt oxide as a highly efficient electrocatalyst for oxygen evolution reaction. *J. Mater. Chem. A* **2019**, *7*, 7526-7532.
31. Xu, H.; Wang, B.; Shan, C.; Xi, P.; Liu, W.; Tang, Y. Ce-Doped NiFe-layered double hydroxide ultrathin nanosheets/nanocarbon hierarchical nanocomposite as an efficient oxygen evolution catalyst. *ACS Appl. Mater.* **2018**, *10*, 6336-6345.
32. Krishna, A.; Sreeremya, T.S.; Ghosh, S. Morphology evolution and growth of cerium oxide nanostructures by virtue of organic ligands as well as monomer concentration. *CrystEngComm.* **2015**, *17*, 7094-7106.
33. Pastor-Perez, L.; Reina, T.R.; Lvanova, S.; Centeno, M.A.; Odriozola, J.A.; Sepulveda-Escribano, A. Ni-CeO₂/C catalysts with enhanced OSC for WGS reaction. *J. Catal.* **2015**, *5*, 298-309.
34. Yan, X.; Tian, L.; Li, K.; Atkins, S.; Zhao, H.; Murowchick, J.; Liu, L.; Chen, X. FeNi₃/NiFeO_x nanohybrids as highly efficient bifunctional electrocatalysts for overall water splitting. *Adv. Mater.* **2016**, *3*, 1600368.
35. Shinagawa, T.; Garcia-Esparza, A.T.; Takanabe, K. Insight on Tafel slopes from a microkinetic analysis of aqueous electrocatalysis for energy conversion. *Sci. Rep.* **2015**, *5*, 13801.